Petroleum Science 20 (2023) 3918–3930

Contents lists available at ScienceDirect

Petroleum Science

journal homepage: www.keaipublishing.com/en/journals/petroleum-science

Original Paper

Three novel dendritic chitosan derivatives for inhibiting acid corrosion of petroleum pipelines

Guo-Dong Cui [a, f], Yan-Ming Chen [b], Qi-Ming Zhang [a], Zheng Wang [a], Tian Tang [a], Qing Zhao [c], Yu Zhang [d], Li-Feng Zhang [d], Yuan-Qi Gu [e], Yang-Sheng Liu [a, *]

[a] College of Environmental Sciences and Engineering, Peking University, Beijing Key Laboratory for Solid Waste Utilization and Management, Beijing, 100871, China
[b] University of Houston, Houston, TX, 77204, United States
[c] State Key Laboratory of Heavy Oil Processing, College of Science, China University of Petroleum, Beijing, 102249, China
[d] CenerTech Tianjin Chemical Research and Design Institute Co., Ltd, China National Offshore Oil Corp (CNOOC) Tianjin, 300131, China
[e] Faculty of Environment and Life, Beijing University of Technology, Beijing, 100124, China
[f] Shanxi International Energy Group Co., Ltd, Taiyuan, 030002, Shanxi, China

ARTICLE INFO

Article history:
Received 22 March 2022
Received in revised form
21 September 2022
Accepted 8 August 2023
Available online 9 August 2023

Edited by Jia-Jia Fei

Keywords:
Chitosan derivatives
Corrosion inhibitors
Carbon steel
Acid inhibition
Efficient and environmental

ABSTRACT

In the process of exploration and development of oil and gas fields, the acidic environment of oil reservoir, production and transport processes cause corrosion of pipelines and equipment, resulting in huge economic losses and production safety risks. Corrosion inhibitors were widely used in oil industry because of simple operation process and economical. In this study, three environmentally friendly corrosion inhibitors were synthesized based on the natural polysaccharide chitosan. Corrosion inhibition of three dendritic chitosan derivatives (We name them BH, CH and DH) on mild steel in 1 mol/L HCl solution with natural ventilation system was evaluated by weight loss experiment, electrochemical analysis and surface morphology characterization. The experimental results showed that when the three dendritic chitosan derivatives added in the corrosive medium were 500 mg L^{-1}, the corrosion inhibition efficiencies were all more than 80%. Based on quantum chemical calculation, inhibition mechanisms of three dendritic chitosan derivatives were investigated according to molecular structures. The results showed that the benzene ring, Schiff base and N atom contained in the molecule were the active centers of electron exchange, which were more likely to form a film on the carbon steel surface, thereby slowing or inhibiting corrosion. The results also predicted the corrosion inhibition effect BH > DH > CH, which was consistent with the experimental conclusion.

1. Introduction

During oil exploitation, oilfield reservoirs contain formation water and carbon dioxide (CO_2) (Stack and Abdulrahman, 2012; Hassani et al., 2014), crude oil contains hydrogen sulfide (H_2S) (Tomin and Silinskaya, 2010; Wang and Zhang, 2016), electrochemical corrosion caused by the surrounding environment (Guo et al., 2015; Liu et al., 2020) and acid waste from acidification operations (Migahed et al., 2016; Ganeeva et al., 2020) will inevitably cause serious corrosion to production equipment (Chen et al., 2021), transportation equipment (Hu et al., 2014) and pipelines (Zhang et al., 2021). According to the Chinese Academy of Engineering research results of "Research on China's Corrosion Status and Control Strategies" in 2015, the annual corrosion cost in China is about RMB 2178.82 billion, accounting for 3.34% of China's GDP in 2014 (Hou, 2019). The main countermeasures include the development of high corrosion resistant composite (Wang et al., 2008), electrochemical protection (Popov and Korzunin, 2012), anti-corrosion coatings (Wang et al., 2015; Li et al., 2022) and corrosion inhibitors. At present, adding corrosion inhibitors is one of the most common methods because of their simple operation and low cost.

At present, a series of corrosion inhibitors have been developed, mainly including inorganic and organic corrosion inhibitors. Inorganic corrosion inhibitors mainly include chromate (Eshaghi and

* Corresponding author.
E-mail address: yshliu@pku.edu.cn (Y.-S. Liu).

https://doi.org/10.1016/j.petsci.2023.08.010

Eshaghi, 2012), phosphate (Yan et al., 2019), silicate (Cheng et al., 2020), molybdate (Ou et al., 2018) and so on. Organic corrosion inhibitors mainly include imidazolines (Jawich et al., 2012), quaternary ammonium salts (Chauhan et al., 2020), Schiff bases and carbonyl compounds (Gao et al., 2009), etc. However, both inorganic and organic corrosion inhibitors are toxic and pollute the environment. The development of low toxicity and environment-friendly corrosion inhibitors is the trend in the future.

In this study, we used the natural polysaccharide chitosan as the base molecule, which is widely sourced, nontoxic and degradable. Three branched chitosan derivatives (BH, CH and DH) were synthesized as environmentally friendly corrosion inhibitors. This type of polysaccharide corrosion inhibitor has a large number of polar groups, which adsorb on the metal surface to form a film, thereby inhibiting corrosion. Using electrochemical tests and weight loss experiments to evaluate inhibition efficiency of the three inhibitors for 20# low carbon steel in 1 mol/L HCl solution. The results indicated that three polysaccharide inhibitors synthesized showed good corrosion inhibition effect. Adsorption of polysaccharide molecules on mild steel was confirmed by SEM, contact angle and quantum calculation, and the action mechanism of corrosion inhibitor was clarified.

2. Experimental

2.1. Materials

In this study, we used 20# steel as the experimental sample, and its element composition was shown in Table 1. The sample size steel is 50 mm × 13.5 mm × 2 mm. Before the experiment, samples were pretreated as follows: Petroleum ether was used to remove grease of the steel samples surface. Then ultrasonic cleaning was carried out in ethanol solution and deionized water successively. Then mild steels were dried under nitrogen atmosphere and weighed.

The chemicals used in this study include methanol, ethanol, petroleum ether, hydrochloric acid (HCl), chitosan oligosaccharide (COS, molecular weight≤5000) were purchased from Beijing Nuobeiwei Technology Co. Ltd. The methyl acrylate (MA), glycidyltrimethyl ammonium chloride (GTMAC), ethylenediamine (EDA), 4-Isopropylaniline, 4-pyridinecarboxaldehyde and 2,2-pyridi were purchased from Sinopharm Chemical Reagent. The corrosive medium was 1 M HCl solution with naturally ventilation.

2.2. Synthesis of branched polymers derivatives

The synthesis route of hyperbranched chitosan oligomer derivatives BH, CH and DH were showed in Fig. 1. Michael addition reaction: chitosan oligosaccharide (5.0 g) and 2.0 mL methyl acrylate were dispersed in methanol. The solution was stirred at 50 °C for 48 h. The precipitation product was obtained by centrifugation at 3.5 × 10^3 rpm and repeatedly washed 3 times. Amidation reaction: The reactants from the previous step were added to 100 mL methanol, then 5 mL ethylenediamine was added to the flask. The mixture was stirred and the solvent and unreacted methyl acrylate were removed by centrifugation. The precipitation product is the first-generation branched chitosan. The michael addition and amidation reactions were repeated to obtain the second-generation branched chitosan. The second-generation branched chitosan (5.0 g) and glycidyl trimethylammonium chloride (5.0 g) were added to 200 mL aqueous solution. The mixture was stirred at 80 °C for 72 h. Product was collected by filtration after extraction with acetone. The products were reacted with NBS (reaction of 4-isopropylaniline with di-2-pyridylethanedione), citral and 4-pyridinecarboxaldehyde in ethanol solution at 70 °C for 7 days to obtain BH, CH and DH.

Table 1
The element composition of 20# carbon steel (mass% balance is Fe).

Element	Composition, %
C	0.17–0.24
Si	0.17–0.37
Mn	0.35–0.65
Cr	≤0.15
P	0.035
S	0.035
Ni	≤0.15

2.3. Weight loss method

Gravimetric method is a method to calculate the corrosion inhibition efficiency by comparing the weight changes of samples before and after corrosion. It is a reliable, simple and widely used experimental method. In order to simulate the acid corrosive environment of the oil field, the formation water contains a large amount of dissolved oxygen. In this study, the corrosive medium we used was 1 M HCl solution with natural ventilation system. The surface area of carbon steel samples was measured to ensure that the addition of corrosive medium (1 M HCl) is not less than 20 mL/cm^2. Carbon steel samples were immersed in 1 M HCl solution with natural ventilation at 60 °C for 7 days. The entire surface of the sample was in complete contact with the corrosive medium, and the sample was not in contact with the vessel wall.

After the test, the samples were taken out and rinsed with deionized water immediately, and then brushed with a soft brush. The samples were dried with cold air, placed in a desiccator for 20 min, and then weighed (accurate to 0.01 mg).

The corrosion rate v_i (mg·(cm^2·h)$^{-1}$) was calculated according to the formula equation:

$$v_i = \frac{\Delta m_i}{A_i \cdot \Delta t} \tag{1}$$

where Δm_i (mg) is corrosion loss of sample, Δt (h) is corrosion time, and A_i (cm^2) is sample surface area, t (h) is the immersion time. The corrosion inhibition rate (IR) is obtained according to the following formula:

$$IR(\%) = \frac{v_{i(\text{blank})} - v_{i(\text{inh})}}{v_{i(\text{blank})}} \times 100 \tag{2}$$

where $v_{i(\text{blank})}$ and $v_{i(\text{inh})}$ are the sample corrosion rates blank and add corrosion inhibitors, respectively.

2.4. Micromorphological analysis

Field emission scanning electron microscope (SEM, Quanta 200 F) was used to observe the changes of carbon steel sample surface microstructure and corrosion products before and after adding corrosion inhibitor to determine the degree of corrosion. In addition, the distribution of corrosion products was determined by energy dispersive spectrometer (EDS). Hydrophobic and hydrophilic performance of the carbon steel sample was obtained by measuring contact angle. Corrosion products produced of carbon steel make the surface uneven and hydrophilic, which means that the surface of carbon steel samples is in more contact with the corrosive medium, resulting in more severe corrosion. If the carbon steel sample surface shows high hydrophobicity, the sample corrosion inhibition ability will be enhanced.

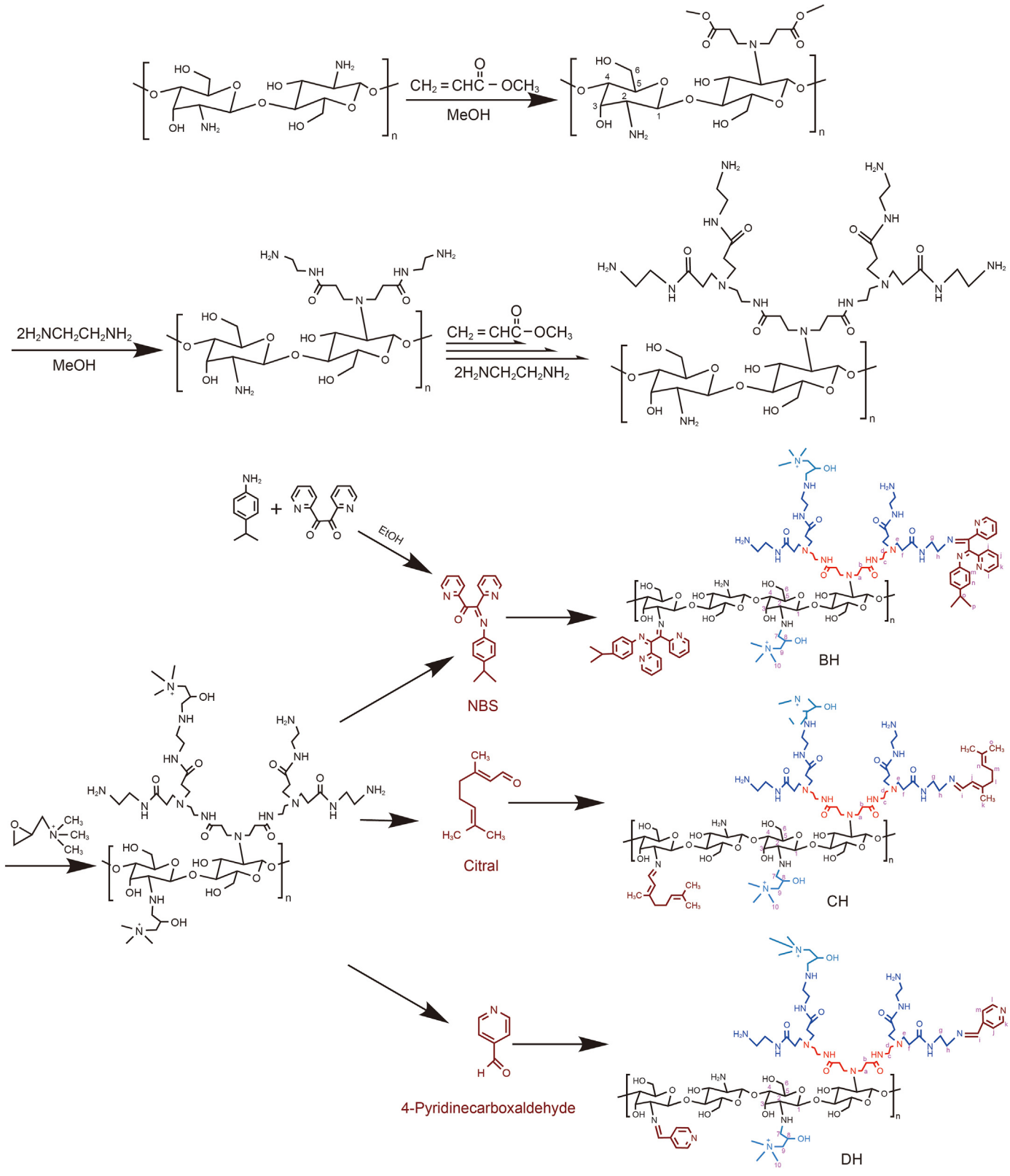

Fig. 1. The synthetic routes of hyperbranched chitosan oligomer derivatives BH, CH and DH.

2.5. Electrochemical testing

The corrosion of metal materials is electrochemical reaction. Metal materials are in contact with electrolyte (corrosive medium), and corrosion is occurred at the electrode. Electrochemical corrosion is a redox reaction. During the reaction, the metal loses electrons and is oxidized, and the corrosive medium gain electrons from the metal surface and are reduced. This process can be studied

by measuring the electrical signals during the corrosion process. Linear polarization curves (Tafel curve) and AC impedance tests are two common methods for studying metal corrosion.

In this study, electrochemical workstation (ch660e, Shanghai, China) was used to measure linear polarization curves and AC impedance during corrosion. The three-electrode system include working electrode (carbon steel with exposed area of 1 cm^2), reference electrode (Ag–AgCl electrode) and counter electrode (platinum metal mesh).

Before the electrochemical test, the open circuit potential (OCP) tests were carried out for 1 h until the potential stabilized. The scanning range of the potentiodynamic polarization curve was OCP ±0.5 V, and the scanning rate was 1 mV/s.

Using the following formula to calculate the corrosion inhibition rate η (%) of the corrosion inhibitor:

$$\eta(\%) = \frac{i_0 - i_{corr}}{i_0} \times 100 \tag{3}$$

where i_0 and i_{corr} are the corrosion current density of blank corrosion and after adding corrosion inhibitor, respectively.

In the AC impedance test, OCP was used as the voltage, the frequency range was from 100 kHz to 0.01 Hz, and the sinusoidal excitation amplitude was 10 mV. Each experiment was repeated three times to ensure the accuracy of the experimental results. ZSimpwin software were used to analyze the test data, calculate the relevant parameters. The corrosion inhibition efficiencies *IE* (%) in the impedance tests were calculated according to the following formula:

$$IE(\%) = \frac{R_{ct} - R_{ct}^0}{R_{ct}} \times 100 \tag{4}$$

where R_{ct} and R_{ct}^0 are the charge transfer resistance of blank corrosion and after adding corrosion inhibitor, respectively.

2.6. Quantum chemical calculations

The corrosion inhibition efficiencies of three branched chitosan derivatives molecules to metal materials depends on their interaction with metal surface. The stronger the interaction force, the easier it is to adsorb on the metal surface, protect metal from contact with corrosive media, and the stronger the corrosion inhibition ability. Based on density functional theory (DFT), the structures of branched chitosan derivatives molecules were optimized, and the lowest unoccupied molecular orbital energy (E_{LUMO}) and highest occupied molecular orbital energy (E_{HOMO}) were calculated. Electron exchange number (ΔN) between the organic structure and the iron atom was calculated by using the following formulas:

$$A = -E_{LUMO} \tag{5}$$

$$I = -E_{HOMO} \tag{6}$$

$$\eta = (I - A)/2 \tag{7}$$

$$\chi = (I + A)/2 \tag{8}$$

$$\Delta N = (\chi_{Fe} - \chi_{inh})/2(\eta_{Fe} + \eta_{inh}) \tag{9}$$

$$\omega = \chi^2 \Big/ 4\eta \tag{10}$$

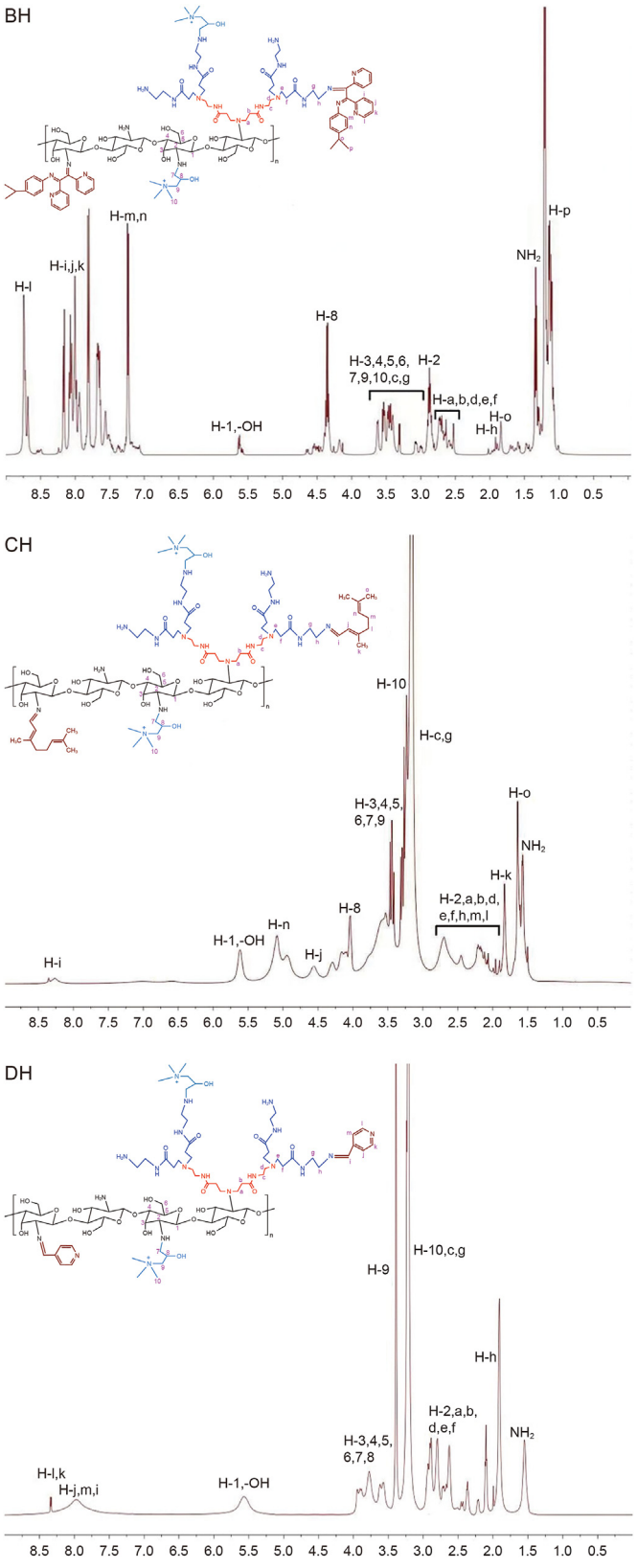

Fig. 2. ^{1}H NMR spectrum of BH, CH and DH (Some pictures are from Cui et al., 2022).

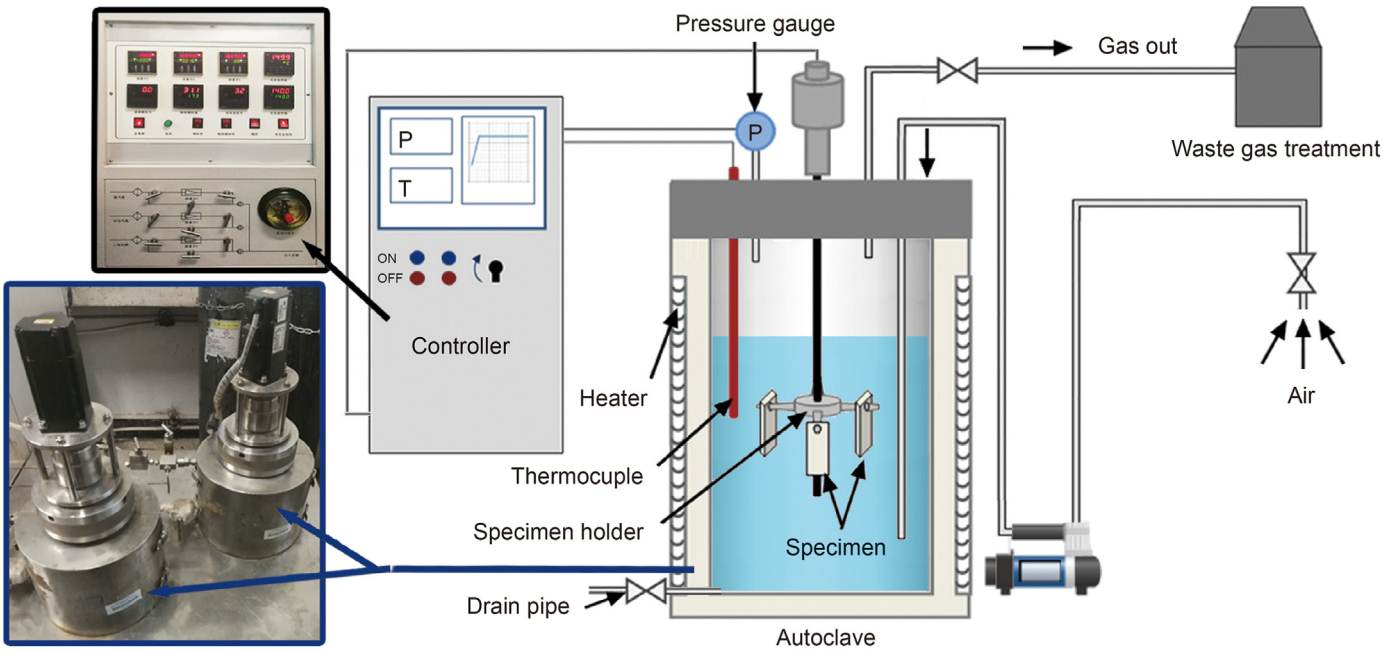

Fig. 3. Weight loss experimental setup diagram.

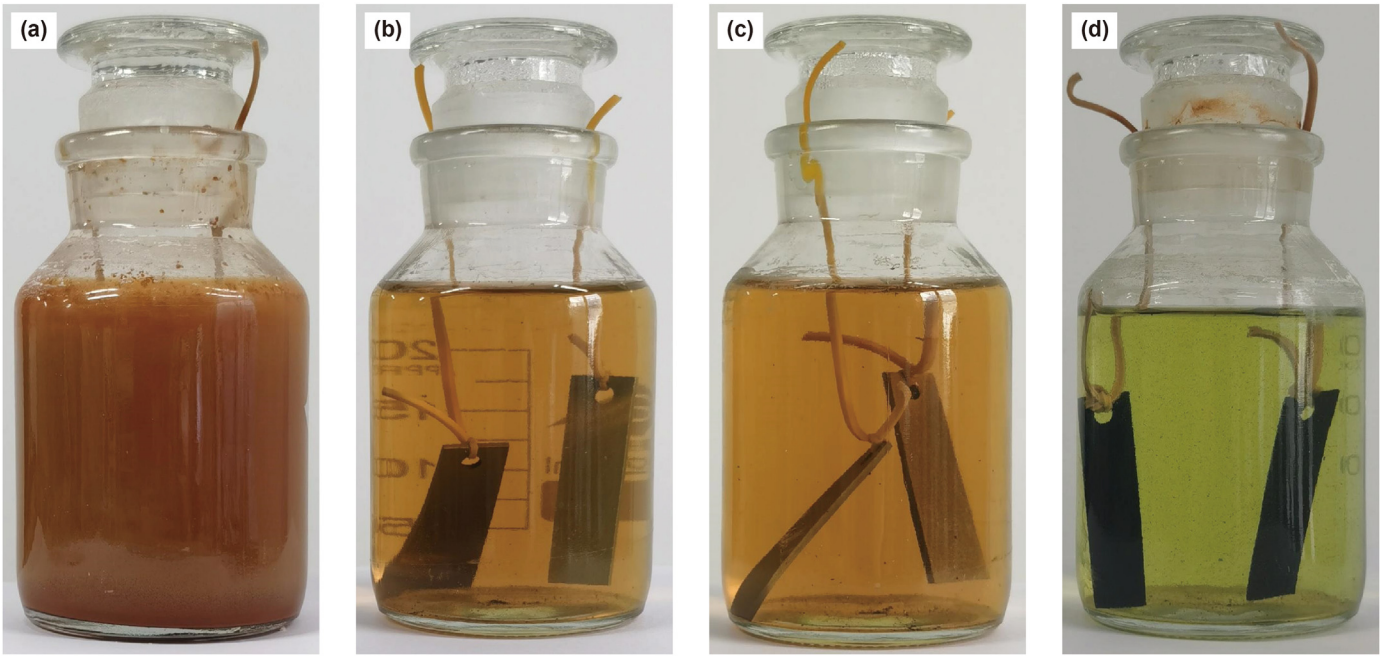

Fig. 4. The solution of 20# carbon steel samples immersed in 1 M·HCl at 60 °C for 7 days.

$$\varepsilon = 1/\omega \tag{11}$$

where A is electron affinity; I is ionization potential, respectively; η is the molecular hardness; χ represents the electronegativity; ΔN is the electrons transferred. χ_{Fe} and χ_{inh} are electronegativities of iron and inhibitors, respectively; η_{Fe} and η_{inh} are iron hardness of iron and inhibitors, respectively; According to the literature (Ahamad et al., 2010; Solmaz, 2014), χ_{Fe} and η_{Fe} are 7.0 and 0 eV, respectively. ω is electrophilic index; ε is nucleophilic index (Obot and Gasem, 2014).

3. Results and discussion

3.1. Chemical characterization

The ^{1}H NMR spectra of branched chitosan derivatives BH, CH and DH were shown in Fig. 2. In ^{1}H NMR spectral curve, δ 1.5–1.7 ppm: NH_2; δ 2.2–3.0 ppm: CH_2 and CH; δ 3.2–3.5 ppm: N–CH_2; 3.30 ppm: N–CH_2; 3.5–3.9 ppm: O–CH. In BH spectrum, δ 7.10–8.20 ppm: aromatic protons; δ 8.73 ppm: pyridine. Similarly. In CH ^{1}H NMR spectrum, δ 5.20 ppm: CH=C; δ 8.26 ppm: CH=N. In DH spectrum, δ 7.95–8.40 ppm: N=CH and pyridine.

Table 2
Weight loss tests for 20# steel in different concentrations of biopolymers in 1 M HCl at various temperatures.

Inhibitor	Conc., mg·L^{-1}	Corrosion rate, mg·(cm^2·h)$^{-1}$				Inhibition efficiency, %			
		30 °C	40 °C	50 °C	60 °C	30 °C	40 °C	50 °C	60 °C
Blank	0	4.62	6.13	9.27	13.46	–	–	–	–
BH	50	1.10	1.56	2.66	4.63	76.19	74.55	71.31	65.60
	100	0.87	1.24	2.08	3.59	81.17	79.77	77.56	73.33
	300	0.63	0.90	1.52	2.64	86.36	85.32	83.60	80.39
	500	0.52	0.73	1.23	2.11	88.74	88.09	86.73	84.32
CH	50	1.61	2.26	3.73	6.37	65.15	63.13	59.76	52.67
	100	1.08	1.53	2.58	4.36	76.62	75.04	72.17	67.61
	300	0.83	1.18	1.92	3.18	82.03	80.75	79.29	76.37
	500	0.68	0.96	1.57	2.53	85.28	84.34	83.06	81.20
DH	50	1.40	1.99	3.35	5.65	69.70	67.53	63.86	58.02
	100	0.95	1.37	2.33	3.96	79.44	77.65	74.87	70.58
	300	0.68	0.94	1.60	2.85	85.28	84.67	82.74	78.83
	500	0.57	0.80	1.34	2.29	87.66	86.95	85.54	82.99

Table 3
The comparative lists of previous reported environment-friendly corrosion inhibitors and present work.

Corrosion inhibitor	Test material	Optimal dosage, mg/L	Corrosion medium and temperature	IE (%) Weight loss
Chitosan-thiosemicarbazide (Chauhan et al., 2018)	Mild steel	200	1 M HCl 35 °C	88.64
O-fumaryl-chitosan (Sangeetha et al., 2016)	Mild steel	500	1 M HCl 25 °C	93.20
Carboxymenthylchitosan (Cheng et al., 2007)	Mild steel	200	1 M HCl 25 °C	93.00
Amino acid ester salts (Aslam et al., 2020)	Mild steel	200	1 M HCl 30 °C	86.19
Bauhinia tomentosa leaves extract (Perumal et al., 2017)	Mild steel	700	1 M HCl 60 °C	69.81
Ondansetron hydrochloride drug (Vengatesh et al., 2017)	Mild steel	300	1 M HCl 60 °C	73.81
Allium Jesdianum extract (Kahkesh and Zargar, 2021)	Mild steel	800	1 M HCl	93.05
Combretum indicum leaf extract (Neriyana and Alva, 2020)	Mild steel	750	1 M HCl 30 °C	82.59
N–hydroxybenzothioamide derivatives (Verma et al., 2021)	Mild steel	300	1 M HCl 55 °C	81.01
Dendritic chitosan [present work]				
BH	Mild steel	500	1 M HCl 60 °C	84.32
CH	Mild steel	500	1 M HCl 60 °C	81.20
DH	Mild steel	500	1 M HCl 60 °C	82.99

3.2. Weight loss experiment

20# carbon steels were used as the experimental samples. Fig. 3 was the experimental setup diagram of the weight loss experiment. Fig. 4 was the solutions of 20# carbon steel sample immersed in 1.0 M HCl at 60 °C and added different inhibitors of the same concentration (500 mg L^{-1}) for 7 days. The corrosions of carbon steel samples were very serious in the corrosion medium without inhibitors after 7 days, and the solution was turbid and orange yellow. The phenomenon was attributed to the corrosion products produced by the corrosion of hydrochloric acid and dissolved oxygen. After 500 mg L^{-1} BH (Fig. 4b), CH (Fig. 4c) and DH (Fig. 4d) corrosion inhibitors were added, the corrosion products were significantly reduced and the solution was clarified, indicating that carbon steel samples corrosion was significantly inhibited.

Table 2 was the experimental results of 20# carbon steel samples measured by weight loss method when adding different concentrations of corrosion inhibitors to 1.0 mol L^{-1} hydrochloric acid solution at various temperatures. The results illustrated that after adding corrosion inhibitor, corrosion rates of samples decreased significantly. With the inhibitor concentration increase, the corrosion rate v_i decrease, the inhibitor efficiency increases. However, with the increase of temperature, the efficiency of corrosion inhibitor decreases, which is attributed to the desorption of the inhibitor adsorption film at high temperature. When concentration of corrosion inhibitors BH, CH and DH in the corrosive medium was 500 mg L^{-1} at 60 °C, the corrosion rate of 20# steel samples decreased from 13.46 mg·(cm^2·h)$^{-1}$ to 2.11, 2.53 and 2.29 mg·(cm^2·h)$^{-1}$ respectively, the corresponding corrosion inhibition efficiencies were 84.32%, 81.20% and 82.99% respectively. At the same inhibitor concentration, the corrosion inhibition efficiency was BH > DH > CH. Table 3 is the comparative lists of previous reported environment-friendly corrosion inhibitors and present work. Compared with other environmentally friendly corrosion inhibitors, chitosan has a wide range of sources and low cost. When the concentration is 500 mg/L in 1 M HCl at 60 °C, the inhibition rates of BH, CH and DH were 84.32%, 81.20%, 82.99%, respectively. Under the same corrosion conditions, the corrosion inhibition rates of Bauhinia tomentosa Leaves (700 mg/L) and Ondansetron hydrochloride drug (300 mg/L) are 69.81% and 73.81% respectively, which is better than most environmentally friendly inhibitors.

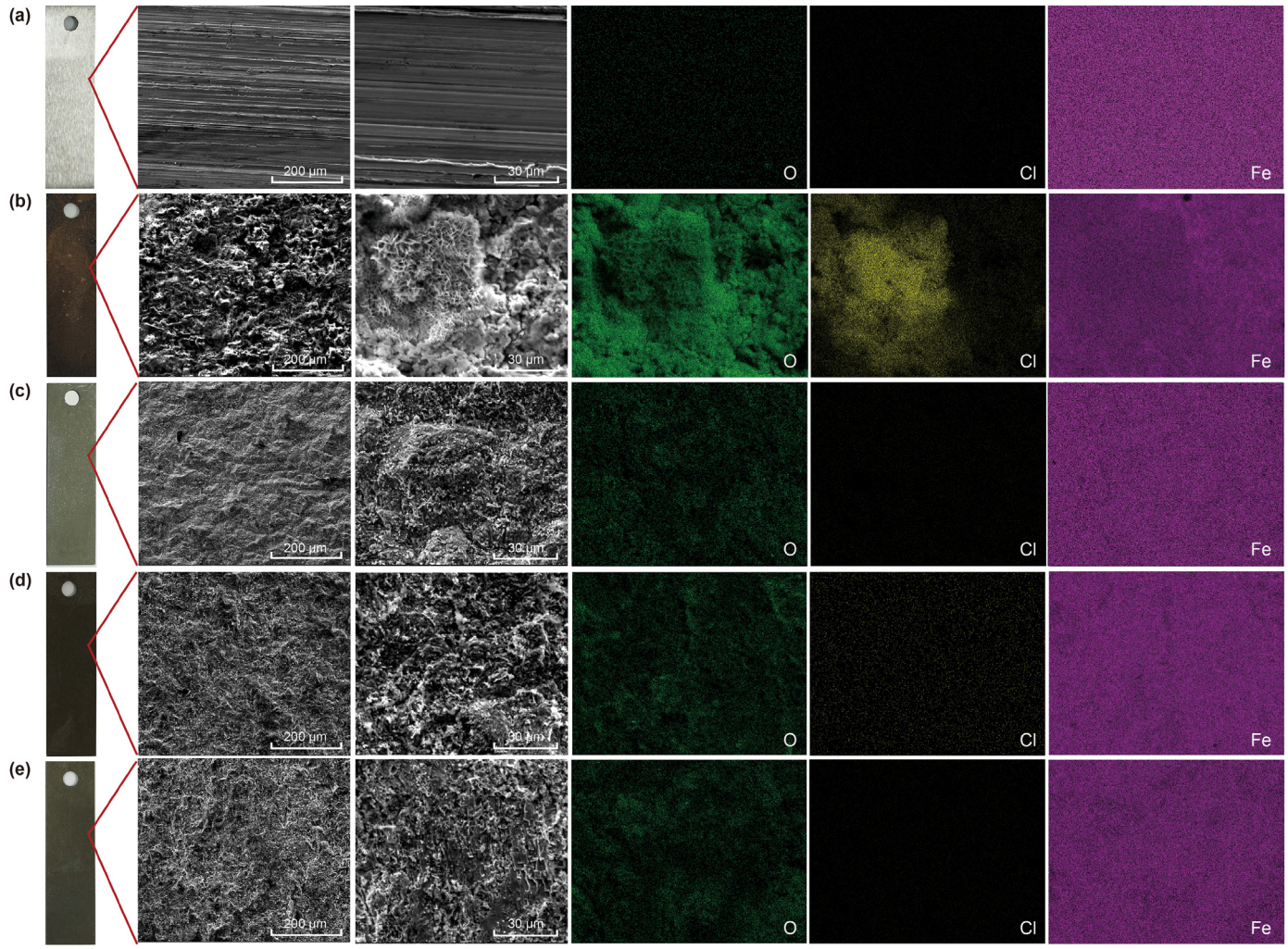

Fig. 5. SEM-EDS analysis in the absence and presence of BH and CH. (**a**) 20# carbon steel sample; (**b**) corrosion without adding inhibitors; (**c**) adding 500 mg L^{-1} BH; (**d**) adding 500 mg L^{-1} CH and (**e**) adding 500 mg L^{-1} DH.

3.3. Surface morphology analysis

3.3.1. SEM-EDS analysis

The inhibition efficiencies of corrosion inhibitors were evaluated by using scanning electron microscope (SEM) to observe the micro morphology of the sample surfaces. The distribution of Cl, O and Fe elements on the sample surface were obtained by energy dispersive spectrum (EDS).

SEM-EDS results of carbon steel samples were shown in Fig. 5. In Fig. 5a, the surface of uncorroded carbon steel sample was smooth and almost no O and Cl elements on the surface, and the Fe element signal was very strong. In Fig. 5b, the surface of the sample without inhibitor was rough. A large amount of O and Cl elements were distributed on the sample surface. It was attributed to that the carbon steel sample was corroded by hydrochloric acid and dissolved oxygen, and the surface was covered with a large amount of corrosion products. Consequently, the signal of Fe element on the surface of the sample was weak. It indicated that the carbon steel sample is seriously corroded. After adding branched chitosan derivatives BH, CH and DH, the surface of the sample tended to be flat and the corrosion products were significantly reduced in Fig. 5c, d and e. The corrosion was obviously inhibited, which could be proved according to the reduction of the distribution density and signal of O and Cl on the sample surface after the addition of corrosion inhibitor. The results of SEM-EDS analysis confirmed that the synthesized branched chitosan derivatives had the effect of inhibiting corrosion.

The SEM cross-sectional morphology and corresponding EDS linear scanning of carbon steel samples corrosion in 1 M HCl solution at 60 °C for 7 d were shown in Fig. 6. The blank corrosion was showed in Fig. 6a. There was a very thick granular corrosion product film on cross section of samples in Fig. 6a, and the thickness of corrosion products layer was 44.65 μm, indicating that the corrosion was very serious. Fig. 6b, c and d were the cross-sections morphology of steel samples after adding 500 mg L^{-1} BH, CH and DH, respectively. The corrosion scale layers were obviously thinner, and the thickness of the corrosion layer decreased to 11.02, 15.01 and 11.97 μm, respectively. Comparing with the uncorroded carbon steel sample, the EDS linear scanning of the corrosion layer showed that Fe content of corrosion layer was reduced significantly, O element content was obviously increased, Cl element content was slightly increased, and C element content basically unchanged. It was attributed to the adsorption of inhibitors BH, CH and DH on the steel surface to form a protective film. The protective film prevented contact between corrosive medium and steel surface, and reduced the corrosion rate. SEM and EDS analysis results showed

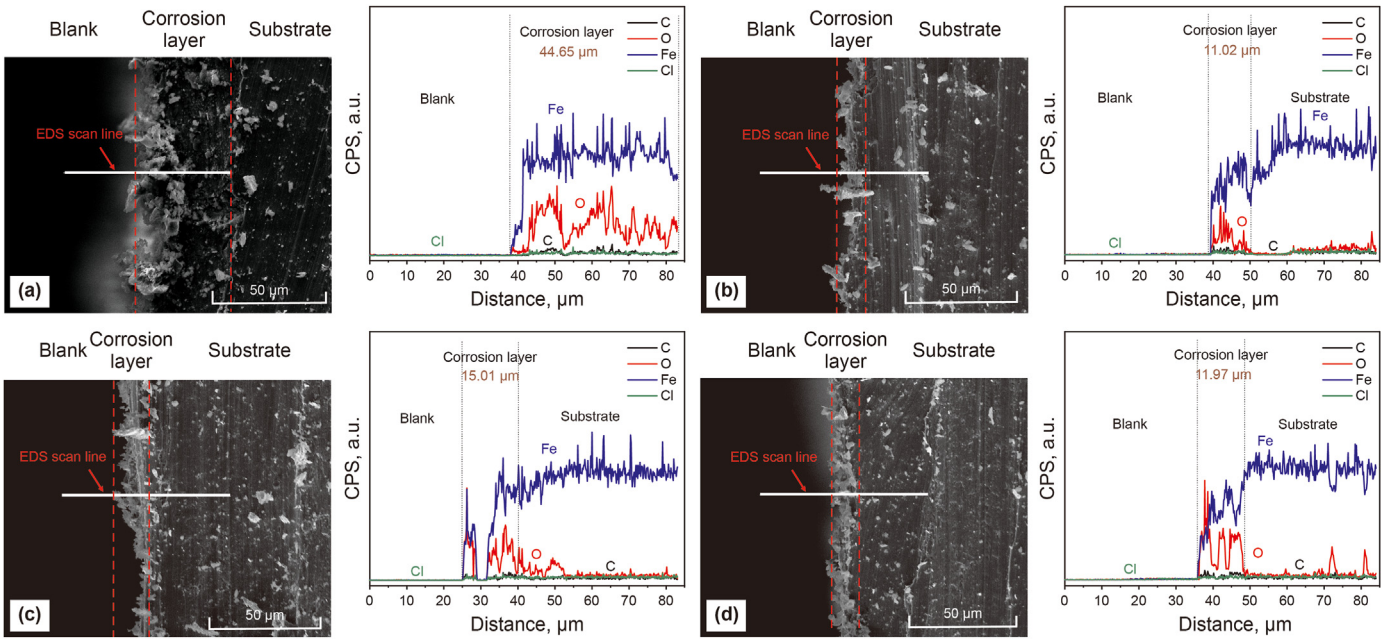

Fig. 6. SEM cross-section morphologies and EDS linear scans of 20# steel after corrosion in 1 M HCl solution at 60 °C for 7 d. (**a**) without inhibitors; (**b**) with 500 mg L^{-1} BH; (**c**) with 500 mg L^{-1} CH and (**d**) with 500 mg L^{-1} DH.

that dendritic chitosan derivatives could effectively inhibit acid medium corrosion of oil pipelines.

3.3.2. Contact angle measurement

The effect of branched chitosan derivatives BH, CH and DH on the hydrophilicity and hydrophobicity of carbon steel surfaces was measured using contact angle tester (Dataphysics, OCA15Pro, Germany). The carbon steel samples contact angle before and after adding corrosion inhibitor was tested, and the results were shown in Fig. 7. For the carbon steel sample without corrosion inhibitor, after being corroded by hydrochloric acid solution, the sample surface was rough and produced a large number of corrosion products, showing high hydrophilicity and a low contact angle (26.5°). The sample surface was more likely to come into contact with the corrosive medium, causing continuous corrosion. After adding corrosion inhibitors, the surface contact angles of carbon steel samples increased, and the surface contact angles of the samples increased 96.4°, 82.3° and 92.3°, respectively. The high hydrophobicity of the sample surface was attributed to that the adsorption films formed by the corrosion inhibitor on the sample surface.

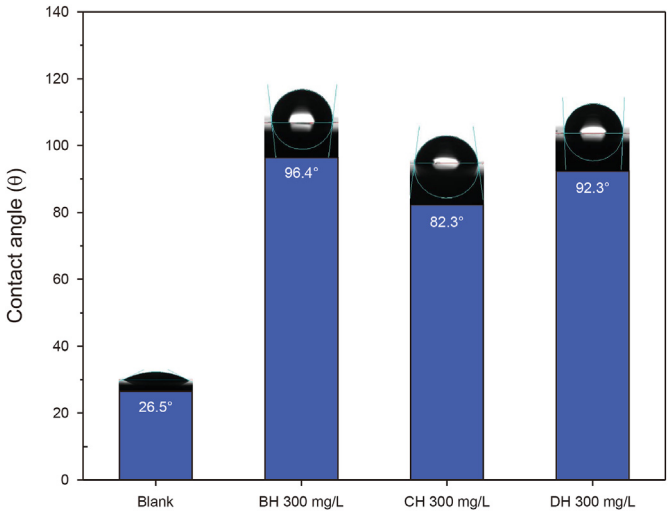

Fig. 7. Contact angle measurements results of carbon steel corrode with inhibitors.

Comparing the molecular structure of three synthetic branched chitosan derivatives, the common hydrophilic groups such as hydroxyl, amino and quaternary ammonium salts can improve the water solubility of polymer molecules, but the molecules also showed higher hydrophilicity, resulting in lower hydrophobicity of the adsorption film formed on the surface of carbon steel. In addition, BH and DH molecules contained benzene ring structure, showing strong hydrophobicity, which could improve the hydrophobicity of the adsorption membrane. The CH molecule had an unsaturated hydrocarbon group, which hydrophobicity was weaker than that of benzene ring structure. Therefore, CH showed low hydrophobicity, and BH and DH showed strong hydrophobicity. After the surface of carbon steel sample was changed from hydrophilic to hydrophobic, it would hinder the contact between the corrosion medium and the carbon steel surface, and prohibited the corrosion rate. The hydrophilicity and hydrophobicity of the sample surface reflected the corrosion inhibition performance of the corrosion inhibitor to a certain extent. The inhibitor with the largest contact angle (the strongest hydrophobicity) showed the better corrosion inhibition performance.

3.4. Electrochemical measurements

The corrosion of carbon steel is an electrochemical process. Electrochemical measurements (potentiodynamic polarization and impedance) can obtain important information such as corrosion rate and the action mechanism of corrosion inhibitor. The electrochemical tests were performed in 1 M HCl solution at 60 °C, which is the same as the experimental conditions of weight loss tests.

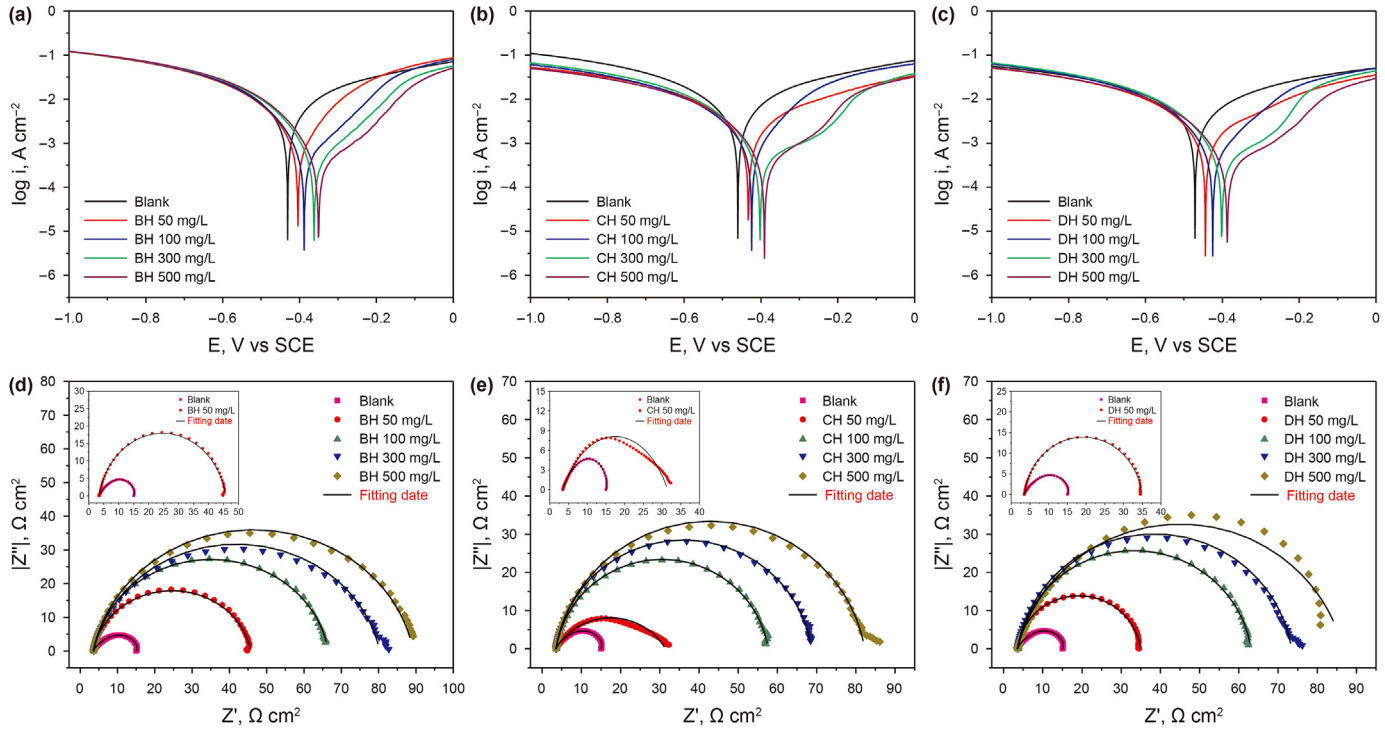

Fig. 8. Tafel and Nyquist curves of various concentrations of BH, CH and DH: (**a**) BH Tafel curves; (**b**) BH Tafel curves; (**c**) BH Tafel curves; (**d**) BH Nyquist curves; (**e**) CH Nyquist curves; (**f**) DH Nyquist curves.

Table 4
Polarization parameters at various concentrations of BH, CH and DH.

Corrosion inhibitor	Concentration, mg·L^{-1}	E_{corr}, mV	i_{corr}, μA/cm	β_c, mV/dec	β_a, mV/dec	η, %
BH	0	−431	4042	−6.061	5.602	
	50	−404	1190	−7.456	9.113	70.56
	100	−388	695.4	−8.363	8.182	82.80
	300	−362	562.8	−8.692	7.467	86.08
	500	−351	503.1	−8.813	6.368	87.55
CH	0	−460	3959	−6.052	5.578	–
	50	−433	1773	−6.048	5.515	55.22
	100	−424	880.4	−6.814	9.203	77.76
	300	−402	704.9	−7.835	3.325	82.19
	500	−391	571.9	−7.440	5.188	85.55
DH	0	−471	3862	−5.070	5.219	–
	50	−444	1631	−6.333	4.361	57.77
	100	−425	738.4	−7.306	8.032	80.88
	300	−401	651.5	−7.874	4.833	83.13
	500	−387	536.2	−7.674	4.492	86.12

Table 5
EIS parameters at different concentrations of BH, CH and DH.

Inhibitors	Concentration, mg·L^{-1}	R_S, Ω·cm^2	R_{ct}, Ω·cm^2	C_{dl}, μF·cm^{-2}	n	IE, %
Blank	0	3.510	12.26	31.48	0.8215	–
BH	50	3.514	42.17	159.04	0.8974	70.93
	100	3.588	62.89	271.04	0.9152	80.51
	300	3.596	76.71	125.22	0.8800	84.02
	500	3.590	85.70	133.68	0.8898	85.69
CH	50	3.478	27.98	13.38	0.7240	56.18
	100	3.594	54.01	272.28	0.9180	77.30
	300	3.552	65.12	217.46	0.9159	81.17
	500	3.560	78.68	130.64	0.8959	84.42
DH	50	3.524	31.37	371.90	0.9330	60.92
	100	3.731	59.34	269.82	0.9158	79.34
	300	3.589	70.23	148.93	0.9055	82.54
	500	3.562	83.02	133.67	0.8562	85.23

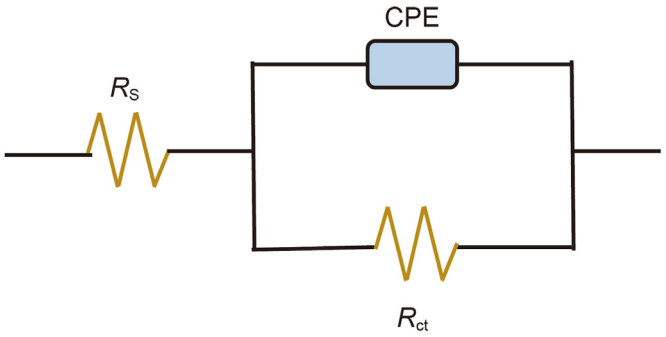

Fig. 9. Electro-equivalent circuit of EIS.

3.4.1. Potentiodynamic polarization testing

Potentiodynamic polarization curves can obtain kinetic information of anodic and cathodic reactions during corrosion of carbon steel samples. Fig. 8a, b and c were the polarization curves of branched chitosan BH, CH and DH in 1 M HCl solution, respectively. The polarization curves of blank corrosion were located at the top of all curves, indicating that corrosion current density was the largest, corrosion rate was the fastest, and corrosion was the most serious. After adding inhibitors, the polarization curves moved down and the corrosion current density decreased, corrosion rate slowed down, and corrosion was inhibited.

Table 4 was the polarization parameters at various concentrations of BH, CH and DH. The corrosion current of carbon steel samples without corrosion inhibitor was 4042 $\mu A \cdot (cm^2)^{-1}$. After adding corrosion inhibitors, corrosion current density decreased greatly. As the inhibitory dose increases, the inhibition efficiency increased. When inhibitors concentration was 500 mg L^{-1}, the inhibition efficiencies of BH, CH and DH were 87.55%, 85.55% and 86.12%, respectively. The efficiencies of three corrosion inhibitors were BH > DH > CH.

3.4.2. Electrochemical impedance spectroscopy measurements

Fig. 8d, e and f were Nyquist curves of corrosion inhibitors BH, CH and DH inhibiting carbon steel corrosion in 1.0 M HCl, respectively. As can be seen from Fig. 8d–f, compared with that without corrosion inhibitor, after adding corrosion inhibitor, the length of the semi major axis of the Nyquist curve increased greatly. With the increased of corrosion inhibitor concentration, this change becomes more and more obvious, which represents the rapid rise of charge transfer resistance R_{ct}, and the electrochemical corrosion of the samples was effectively inhibited. The fitted curve parameters were shown in Table 5. In the blank corrosion experiment, the charge transfer resistance R_{ct} of the corrosion system was 12.26 Ω cm^2. When the inhibitor was added, the R_{ct} increased significantly. When inhibitor concentration reached 500 mg L^{-1}, the R_{ct} of the three inhibitors reached the maximum values, which were 85.70, 78.68 and 83.02 Ω cm^2 respectively, and the corresponding corrosion inhibition efficiencies were 85.69%, 84.42% and 85.23% respectively. It indicated that branched chitosan derivatives could effectively inhibit hydrochloric acid corrosion. Fig. 9 was the circuit used to fit the EIS data. The equivalent circuit consists of solution resistance (R_S), charge transfer resistance (R_{ct}) and constant phase element (CPE).

3.5. Quantum chemical calculations

3.5.1. Molecular orbital calculation

Based on density functional theory (DFT), we investigated the influence of BH, CH and DH molecular structure on interaction force with metal surface. The structures of corrosion inhibitor molecules were optimized. Molecular structural units, optimization structure and orbital distribution of BH, CH and DH were shown in Fig. 10. The relevant quantum chemical calculation parameters of the three corrosion inhibitor molecules BH, CH and DH structural units were shown in Table 6.

The energy gap value (ΔE) is the energy required for electrons to transition and represents the molecular reactivity. The smaller the energy gap value ΔE, the higher the reactivity. According to Table 6, $\Delta E_{BH\text{-}2\text{-}Unit} < \Delta E_{BH\text{-}1\text{-}Unit} < \Delta E_{CH\text{-}2\text{-}Unit} < \Delta E_{DH\text{-}2\text{-}Unit} < \Delta E_{CH\text{-}1\text{-}Unit} < \Delta E_{DH\text{-}1\text{-}Unit} < \Delta E_{Common\text{-}Unit}$, and BH-2-Unit showed the highest reactivity. ΔN is the electron exchange number between the inhibitor molecule and the iron atom, $\Delta N_{BH\text{-}1\text{-}Unit} > \Delta N_{CH\text{-}1\text{-}Unit} > \Delta N_{BH\text{-}2\text{-}Unit} > \Delta N_{CH\text{-}2\text{-}Unit} > \Delta N_{DH\text{-}2\text{-}Unit} > \Delta N_{DH\text{-}1\text{-}Unit} > \Delta N_{Common\text{-}Unit}$. The BH-1-Unit showed the highest reactivity.

In addition, electrophilic index (ω) of each structural unit were analyzed. The higher the ω value, the easier it is to accept electrons. Iron, as a metal atom, tends to lose electrons, so molecular structures that easily acquire electrons are more likely to interact with iron. According to Table 6, $\omega_{BH\text{-}2\text{-}Unit} > \omega_{Common\text{-}Unit} > \omega_{CH\text{-}2\text{-}Unit} > \omega_{BH\text{-}1\text{-}Unit} > \omega_{DH\text{-}2\text{-}Unit} > \omega_{DH\text{-}1\text{-}Unit} > \omega_{CH\text{-}1\text{-}Unit}$, indicating that BH-2-Unit structural unit is most likely to interact with iron. Based on orbital calculations, BH molecule showed low energy gap ΔE, higher ΔN, and strong electrophilicity ω. Therefore, it was speculated that BH had the best corrosion inhibition effect. This was basically consistent with the conclusion of the experiment.

3.5.2. Active site analysis

According to the optimized structure and orbital parameters of the inhibitor molecule, the Fukui index of the atoms in the inhibitor molecule could be obtained by calculation, and the electrophilic and nucleophilic properties of each atom in the inhibitor molecule could be predicted.

Fig. 11 was the atoms with higher f_k^+ and f_k^- Fukui index values in molecular structural units. Atoms with higher f_k^+ values will be more inclined to as active sites for accepting electrons, and atoms with higher f_k^- will be more likely as active sites for donating electrons. Comparing the distribution of active sites and frontier orbitals, most of the electron-accepting active sites were distributed in the LUMO region, and the electron donors were distributed in the HOMO region. The distribution of active sites was roughly consistent with the distribution of molecular frontier orbitals. When the structural units contain benzene rings, Shiff base and N atoms, the active sites of electron exchange tend to be concentrated to the benzene rings, Shiff base and regions containing N atoms. These regions were more likely to interact with iron atoms, which confirmed that the corrosion inhibitor with benzene rings, Shiff base and N atoms showed better corrosion inhibition performance from the molecular point of view.

4. Conclusions

Three novel dendritic chitosan derivatives, BH, CH and DH were successfully synthesized as environment-friendly corrosion inhibitors. The corrosion inhibition performances of dendritic chitosan were studied through weight loss experiment, surface morphology characterization and electrochemical tests. It indicated that three corrosion inhibitors showed good corrosion inhibition efficiency. When concentration of corrosion inhibitors BH, CH and DH in 1 M HCl was 500 mg L^{-1} at 60 °C, the corresponding highest corrosion inhibition efficiencies were 87.55%, 85.55% and 86.12% respectively. SEM-EDAX analysis results indicated that after adding dendritic chitosan derivatives, the carbon steel surface became flat, the corrosion products were significantly reduced, and the

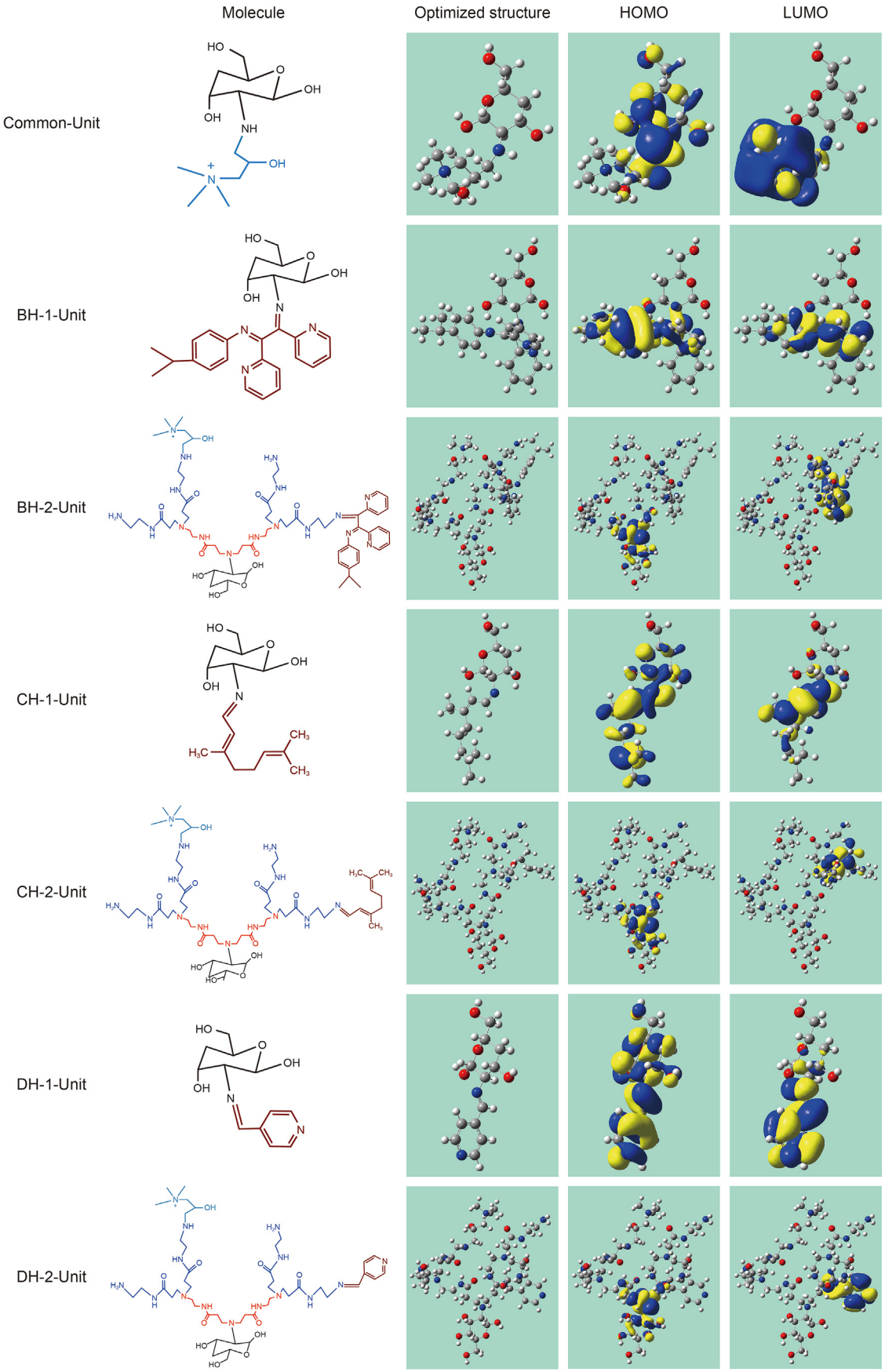

Fig. 10. Optimal structure and orbital distribution of structural units of BH, CH and DH (Cui et al., 2022).

Table 6
Quantum chemistry calculation parameters of BH and CH structural units.

Molecules	E_{HOMO}, eV	E_{LUMO}, eV	ΔE	χ	η	ω	ε	ΔN
Common -Unit	−8.985	−2.455	6.530	5.720	3.265	2.505	0.399	0.196
BH-1-Unit	−6.007	−2.029	3.978	4.018	1.989	2.029	0.493	0.750
BH-2-Unit	−6.485	−2.684	3.799	4.585	1.901	2.765	0.362	0.635
CH-1-Unit	−6.117	−1.076	5.041	3.597	2.521	1.283	0.779	0.675
CH-2-Unit	−6.504	−2.066	4.438	4.285	2.219	2.069	0.483	0.612
DH-1-Unit	−6.758	−1.495	5.263	4.127	2.632	1.618	0.618	0.546
DH-2-Unit	−6.535	−2.007	4.528	4.271	2.264	2.014	0.496	0.603

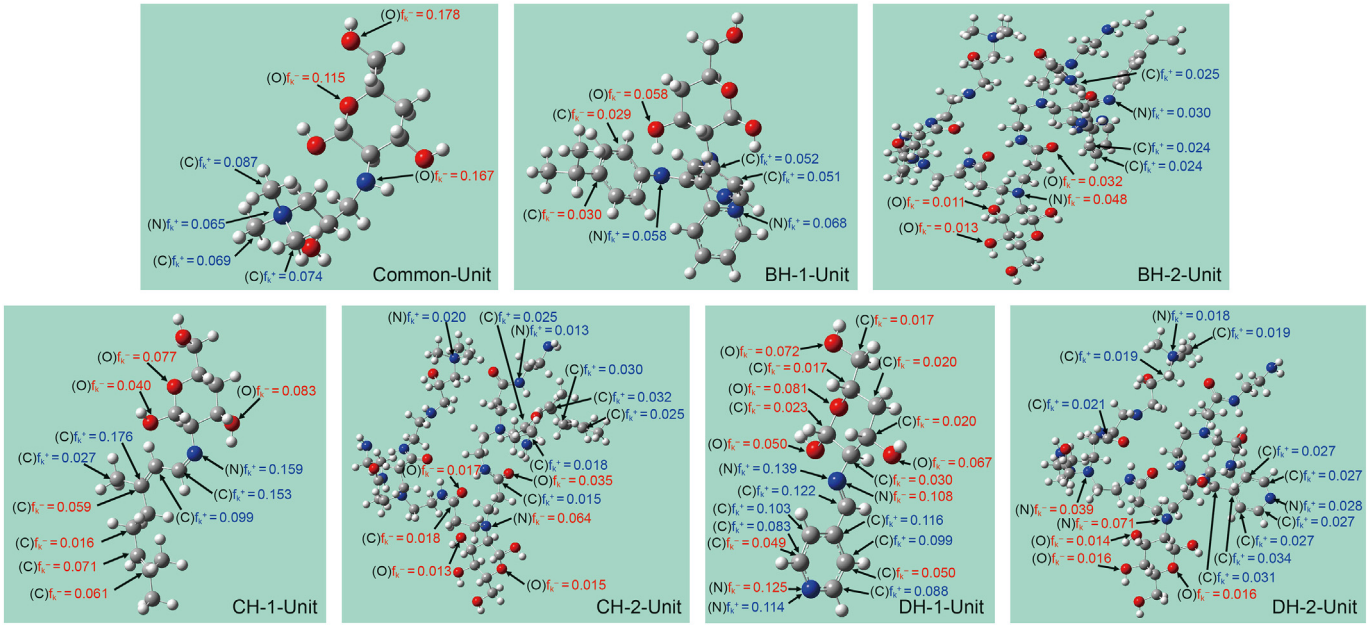

Fig. 11. Active sites of inhibitor molecular structural units.

corrosion was significantly inhibited.

When the same amount of dendritic chitosan derivatives was added, the inhibition efficiencies were BH > DH > CH. After adding three corrosion inhibitors of 500 mg L^{-1} to the corrosive medium respectively, three branched chitosan inhibition efficiencies were all more than 80%. In addition, quantum chemical calculation results of three corrosion inhibitors molecular structures indicated that, BH molecule showed low energy gap ΔE, higher ΔN, stronger electrophilicity ω, and more active sites. BH molecule was more likely to interact with mild steel and form resistance protective film on the samples, and shows higher corrosion inhibition performance. The results are basically consistent with the results obtained by weight loss experiment, surface morphology characterization and electrochemical tests.

Declaration of competing interest

The authors declare that they have no known competing financial interests or personal relationships that could have appeared to influence the work reported in this paper.

Acknowledgements

The authors gratefully acknowledge the College of Environmental Sciences and Engineering, Peking University for providing chemicals and materials research facilities. This research did not receive any specific grant from funding agencies in the public. The authors declare that there are no known competitive relationships and economic conflicts of interest in this paper.

References

Ahamad, I., Prasad, R., Quraishi, M.A., 2010. Experimental and quantum chemical characterization of the adsorption of some Schiff base compounds of phthaloyl thiocarbohydrazide on the mild steel in acid solutions. Mater. Chem. Phys. 124 (2), 1155–1165. https://doi.org/10.1016/j.matchemphys.2010.08.051.

Aslam, R., Mobin, M., Huda, Obot, I.B., Alamri, A.H., 2020. Ionic liquids derived from α-amino acid ester salts as potent green corrosion inhibitors for mild steel in 1 M HCl. J. Mol. Liq. 318, 113982. https://doi.org/10.1016/j.molliq.2020.113982.

Chauhan, D.S., Ansari, K.R., Sorour, A.A., Quraishi, M.A., Lgaz, H., Salghi, R., 2018. Thiosemicarbazide and thiocarbohydrazide functionalized chitosan as eco-friendly corrosion inhibitors for carbon steel in hydrochloric acid solution. Int. J. Biol. Macromol. 107 (Pt B), 1747–1757. https://doi.org/10.1016/j.ijbiomac.2017.10.050.

Chauhan, D.S., Quraishi, M.A., Jafar, Mazumder, M.A., Ali, S.A., Aljeaban, N.A., Alharbi, B.G., 2020. Design and synthesis of a novel corrosion inhibitor embedded with quaternary ammonium, amide and amine motifs for protection of carbon steel in 1 M HCl. J. Mol. Liq. 317, 113917. https://doi.org/10.1016/j.molliq.2020.113917.

Chen, S.S., Wang, H.X., Jiang, H., Liu, Y.N., Liu, Y.X., Lv, X.X., 2021. Risk assessment of corroded casing based on analytic hierarchy process and fuzzy comprehensive evaluation. Petrol. Sci. 18 (2), 591–602. https://doi.org/10.1007/s12182-020-00507-0.

Cheng, S., Chen, S., Liu, T., Chang, X.T., Yin, Y.S., 2007. Carboxymenthylchitosan as an ecofriendly inhibitor for mild steel in 1 M HCl. Mater. Lett. 61 (14), 3276–3280. https://doi.org/10.1016/j.matlet.2006.11.102.

Cheng, L., Lou, F., Guo, W., 2020. Corrosion protection of the potassium silicate conversion coating. Vacuum 176, 109325. https://doi.org/10.1016/j.vacuum.2020. 109325.

Cui, G.D., Zhang, Q.M., Zhao, Q., Wang, Z., Tang, T., He, X., Cui, S., Li, X., Liu, Y.S., 2022. Synthesis of branched chitosan derivatives for demulsification and steel anti-

corrosion performances investigation. Colloids Surf. A Physicochem. Eng. Asp. 653, 130038. https://doi.org/10.1016/j.c olsurfa.2022.130038.
Eshaghi, A., Eshaghi, A., 2012. Effect of chromate conversion coatings on the adhesion and corrosion resistance of painted 5083 aluminum alloy. Mater. Sci. 48 (2), 171–175. https://doi.org/10.1007/s11003-012-9487-9.
Ganeeva, Y.M., Yusupova, T.N., Barskaya, E.E., Valiullova, A.K., Okhotnikova, E.S., Morozov, V.I., Davletshina, L.F., 2020. The composition of acid/oil interface in acid oil emulsions. Petrol. Sci. 17 (5), 1345–1355. https://doi.org/10.1007/s12182-020-00447-9.
Gao, J.C., Weng, Y.J., Salitanate, W., Li, F., Hong, Y., 2009. Corrosion inhibition of α,β-unsaturated carbonyl compounds on steel in acid medium. Petrol. Sci. 6 (2), 201–207. https://doi.org/10.1007/s12182-009-0032-x.
Guo, Y.B., Liu, C., Wang, D.G., Liu, S.H., 2015. Effects of alternating current interference on corrosion of X60 pipeline steel. Petrol. Sci. 12 (2), 316–324. https://doi.org/10.1007/s12182-015-0022-0.
Hassani, S., Vu, T.N., Rosli, N.R., Esmaeely, S.N., Choi, Y.S., Young, D., Nesic, S., 2014. Wellbore integrity and corrosion of low alloy and stainless steels in high pressure CO_2 geologic storage environments: an experimental study. Int. J. Greenh. Gas Control 23, 30–43. https://doi.org/10.1016/j.ijggc.2014.01.016.
Hou, B., 2019. The Cost of Corrosion in China. Springer Singapore Pte, Beijing. Singapore. https://doi.org/10.1007/978-981-32-9354-0 (in Chinese).
Hu, X., Zhou, C., Duan, M., An, C., 2014. Reliability analysis of marine risers with narrow and long corrosion defects under combined loads. Petrol. Sci. 11 (1), 139–146. https://doi.org/10.1007/s12182-014-0325-6.
Jawich, M.W.S., Oweimreen, G.A., Ali, S.A., 2012. Heptadecyl-tailed mono- and bis-imidazolines: a study of the newly synthesized compounds on the inhibition of mild steel corrosion in a carbon dioxide-saturated saline medium. Corrosion Sci. 65, 104–112. https://doi.org/10.1016/j.corsci.2012.08.001.
Kahkesh, H., Zargar, B., 2021. Corrosion protection evaluation of Allium Jesdianum as a novel and green source inhibitor for mild steel in 1 M HCl solution. J. Mol. Liq. 344, 117768. https://doi.org/10.1016/j.molliq.2021.117768.
Li, S., Wang, S., Du, X., Wang, H.B., Cheng, X., Du, Z.L., 2022. Waterborne polyurethane coating based on tannic acid functionalized Ce-MMT nanocomposites for the corrosion protection of carbon steel. Prog. Org. Coating 163, 106613. https://doi.org/10.1016/j.porgcoat.2021.106613.
Liu, H., Dai, Y., Cheng, Y.F., 2020. Corrosion of underground pipelines in clay soil with varied soil layer thicknesses and aerations. Arab. J. Chem. 13 (2), 3601–3614. https://doi.org/10.1016/j.arabjc.2019.11.006.
Migahed, M.A., Zaki, E.G., Shaban, M.M., 2016. Corrosion control in the tubing steel of oil wells during matrix acidizing operations. RSC Adv. 6 (75), 71384–71396. https://doi.org/10.1039/c6ra12835a.
Neriyana, P.S., Alva, V.D.P., 2020. A green approach: evaluation of combretum indicum (CI) leaf extract as an eco-friendly corrosion inhibitor for mild steel in 1 M HCl. Chemistry Africa 3 (4), 1087–1098. https://doi.org/10.1007/s42250-020-00190-z.
Obot, I.B., Gasem, Z.M., 2014. Theoretical evaluation of corrosion inhibition performance of some pyrazine derivatives. Corrosion Sci. 83, 359–366. https://doi.org/10.1016/j.corsci.2014.03.008.
Ou, H.H., Tran, Q.T.P., Lin, P.H., 2018. A synergistic effect between gluconate and molybdate on corrosion inhibition of recirculating cooling water systems. Corrosion Sci. 133, 231–239. https://doi.org/10.1016/j.corsci.2018.01.014.
Perumal, S., Muthumanickam, S., Elangovan, A., Karthik, R., kannan, R.S., Mothilal, K.K., 2017. Bauhinia tomentosa Leaves extract as green corrosion inhibitor for mild steel in 1 M HCl medium. Journal of Bio- and Tribo- Corrosion 3 (2), 1–10. https://doi.org/10.1007/s40735-017-0072-5.
Popov, V.A., Korzunin, G.S., 2012. The experience from using stretched flexible anodes in the system of electrochemical corrosion protection of main gas pipelines. Russ. J. Nondestr. Test. 48 (3), 176–183. https://doi.org/10.1134/S1061830912010 07X.
Sangeetha, Y., Meenakshi, S., Sundaram, C.S., 2016. Interactions at the mild steel acid solution interface in the presence of O-fumaryl-chitosan: electrochemical and surface studies. Carbohydr. Polym. 136, 38–45. https://doi.org/10.1016/j.carbpol.2015.08.057.
Solmaz, R., 2014. Investigation of adsorption and corrosion inhibition of mild steel in hydrochloric acid solution by 5-(4-Dimethylaminobenzylidene)rhodanine. Corrosion Sci. 79, 169–176. https://doi.org/10.1016/j.corsci.2013.11.001.
Stack, M.M., Abdulrahman, G.H., 2012. Mapping erosion–corrosion of carbon steel in oil–water solutions: effects of velocity and applied potential. Wear 274–275, 401–413. https://doi.org/10.1016/j.wear.2011.10.008.
Tomin, V.P., Silinskaya, Y.N., 2010. Corrosion in processes of deep destructive crude-oil processing. Prot Met Phys Chem 46 (7), 758–762. https://doi.org/10.1134/S207020511007004X.
Vengatesh, G., Karthik, G., Sundaravadivelu, M., 2017. A comprehensive study of ondansetron hydrochloride drug as a green corrosion inhibitor for mild steel in 1 M HCl medium. Egyptian journal of petroleum 26 (3), 705–719. https://doi.org/10.1016/j.ejpe.2016.10.011.
Verma, D.K., Kazi, M., Alqahtani, M.S., Syed, R., Berdimurodov, E., Kaya, S., Salim, R., Asatkar, A., Haldhar, R., 2021. N–hydroxybenzothioamide derivatives as green and efficient corrosion inhibitors for mild steel: experimental, DFT and MC simulation approach. J. Mol. Struct. 1241, 130648. https://doi.org/10.1016/j.molstruc.2021.130648.
Wang, Z.M., Zhang, J., 2016. Corrosion of multiphase flow pipelines: the impact of crude oil. Corrosion Rev. 34 (1–2), 17–40. https://doi.org/10.1515/corrrev-2015-0053.
Wang, X.T., Duan, J.Z., zhang, J., Hou, B.R., 2008. Alloy elements' effect on anti-corrosion performance of low alloy steels in different sea zones. Mater. Lett. 62 (8–9), 1291–1293. https://doi.org/10.1016/j.matlet.2007.08.033.
Wang, L., Zong, Q., Sun, W., Yang, Z.Q., Liu, G.C., 2015. Chemical modification of hydrotalcite coating for enhanced corrosion resistance. Corrosion Sci. 93, 256–266. https://doi.org/10.1016/j.corsci.2015.01.033.
Yan, G., Wang, M.Y., Sun, T., Li, X.P., Yin, W.S., 2019. Anti-corrosion property of glass flake reinforced chemically bonded phosphate ceramic coatings. Materials 12 (13), 2082. https://doi.org/10.3390/ma12132082.
Zhang, Z.W., Wang, J.C., Zhang, J.H., Cheng, Y.F., 2021. Modeling of the mechano-electrochemical effect at corrosion defect with varied inclinations on oil/gas pipelines. Petrol. Sci. 18 (5), 1520–1529. https://doi.org/10.1016/j.petsci.2021.08.012.